Available online at www.sciencedirect.com
SCIENCE DIRECT
ELSEVIER
Icarus 172 (2004) 127–140
ICARUS
www.elsevier.com/locate/icarus

Cassini observations of Io's visible aurorae

Paul Geissler [a,*], Alfred McEwen [b], Carolyn Porco [c,1], Darrell Strobel [d], Joachim Saur [e], Joseph Ajello [f], Robert West [f]

[a] *US Geological Survey, 2255 N. Gemini Dr., Flagstaff, AZ 86001, USA*
[b] *Lunar and Planetary Laboratory, University of Arizona, Tucson, AZ 85721, USA*
[c] *Department of Space Sciences, Southwest Research Institute, 1050 Walnut Street, Suite 400, Boulder, CO 80302, USA*
[d] *Department of Earth and Planetary Sciences, Johns Hopkins University, 3400 North Charles Street, Baltimore, MD 21218, USA*
[e] *Applied Physics Laboratory, Johns Hopkins University, 11100 Johns Hopkins Rd., Laurel, MD 20723, USA*
[f] *Jet Propulsion Laboratory, California Institute of Technology, 4800 Oak Grove Drive, Pasadena, CA 91109, USA*

Received 12 May 2003; revised 26 November 2003

Available online 27 March 2004

Abstract

More than 500 images of Io in eclipse were acquired by the Cassini spacecraft in late 2000 and early 2001 as it passed through the jovian system en route to Saturn (Porco et al., 2003, Science 299, 1541–1547). Io's bright equatorial glows were detected in Cassini's near-ultraviolet filters, supporting the interpretation that the visible emissions are predominantly due to molecular SO_2. Detailed comparisons of laboratory SO_2 spectra with the Cassini observations indicate that a mixture of gases contribute to the equatorial emissions. Potassium is suggested by new detections of the equatorial glows at near-infrared wavelengths from 730 to 800 nm. Neutral atomic oxygen and sodium are required to explain the brightness of the glows at visible wavelengths. The molecule S_2 is postulated to emit most of the glow intensity in the wavelength interval from 390 to 500 nm. The locations of the visible emissions vary in response to the changing orientation of the external magnetic field, tracking the tangent points of the jovian magnetic field lines. Limb glows distinct from the equatorial emissions were observed at visible to near-infrared wavelengths from 500 to 850 nm, indicating that atomic O, Na, and K are distributed across Io's surface. Stratification of the atmosphere is demonstrated by differences in the altitudes of emissions at various wavelengths: SO_2 emissions are confined to a region close to Io's surface, whereas neutral oxygen emissions are seen at altitudes that reach up to 900 km, or half the radius of the satellite. Pre-egress brightening demonstrates that light scattered into Jupiter's shadow by gases or aerosols in the giant planet's upper atmosphere contaminates images of Io taken within 13 minutes of entry into or emergence from Jupiter's umbra. Although partial atmospheric collapse is suggested by the longer timescale for post-ingress dimming than pre-egress brightening, Io's atmosphere must be substantially supported by volcanism to retain auroral emissions throughout the duration of eclipse.

Keywords: Io; Aurorae; Satellites; Atmospheres

1. Introduction

Io is the only moon in the Solar System known to display visible atmospheric emissions that are bright enough to be seen with the naked eye. At intensities that reach hundreds of kiloRayleighs (kR), Io's aurorae would appear as bright as moonlit cumulus clouds to an observer on the surface of the satellite. Similar to the aurorae on Earth and other planets, Io's emissions are produced by electron impact excitation of various gases in Io's tenuous atmosphere. First imaged by the Voyager 1 spacecraft while the moon was eclipsed by Jupiter (Cook et al., 1981), little was known about Io's visible aurora until the arrival of the Galileo Orbiter in late 1995 (Belton et al., 1996). Galileo eclipse pictures showed a colorful display of red, greenish and blue glows believed to be due to both atomic and molecular emissions (Geissler et al., 1999). Ground-based telescopic (Scherb and Smyth, 1993; Bouchez et al., 2000; Oliversen et al., 2001) and Hubble Space Telescope (HST) observations (Trauger et al., 1997; Retherford et al., 1999; Oliversen et al., 2000) helped identify the gases and determine the morphology and time-

* Corresponding author.
E-mail address: pgeissler@usgs.gov (P. Geissler).
[1] Now at Space Science Institute, 4750 Walnut Street, Suite 205, Boulder, Colorado 80301, USA.

0019-1035/$ – see front matter
doi:10.1016/j.icarus.2004.01.008

variability of the atomic emissions. In December 2000, the Cassini spacecraft made a gravity-assist pass by Jupiter en route to Saturn and over a week-long period observed 3 complete eclipses of Io through a variety of spectral filters. Initial analysis of those observations (Porco et al., 2003) confirmed previously seen visible emissions tracking the tangent points of the magnetic field to the surface of Io, and detected new emissions in the ultraviolet and near-IR. The ultraviolet emissions were restricted to the deep atmosphere, and the near-IR emissions arose from a distended tenuous atmosphere surrounding the satellite. Here we report more detailed analysis of Cassini's multispectral imaging observations of Io's eclipses. With its fully functioning high-gain antenna, near-ultraviolet sensitivity and better spectral resolution, Cassini was able to fill many of the gaps in our knowledge of these mysterious phenomena.

Earlier observations raised several questions concerning the visible emissions. Galileo violet filter (380–445 nm) images showed bright glows along the equator of Io near the sub-Jupiter and anti-Jupiter points that are similar in morphology to far-ultraviolet emissions from atomic oxygen (OI 135.6 nm) and sulfur (SI 190.0 nm) seen by HST (Roesler et al., 1999). However, no atomic lines have been identified to explain the short-wavelength visible equatorial glows and it was suspected that they are produced by molecular sulfur dioxide fluorescence. Also uncertain is the source of the currents that cause the visible glows. The brightest far-ultraviolet emissions can be seen to periodically shift in latitude, tracking the tangent points of the jovian magnetic field lines (Roesler et al., 1999; Retherford et al., 2000). This should be expected if they are controlled by electrodynamic interactions with the plasma torus (e.g., Saur et al., 2000). In contrast, the visible emissions are often brightest around actively venting volcanoes rather than faithfully following the magnetic field, although analysis of the full Galileo clear-filter data set suggested that the visible emissions tended on average to track the tangent points of the field lines (Geissler et al., 2001). Finally, two pairs of images from two eclipses acquired during Galileo's 15th orbit showed that the disk-averaged brightness dramatically diminished with time elapsed in eclipse (Geissler et al., 1999), suggesting collapse of Io's sublimation-driven atmosphere. However, the limited downlink available from Galileo afforded only snapshots of Io near the start of these eclipses, making interpretation of the brightness variations difficult.

More than 500 images were acquired by the Narrow Angle Camera of Cassini's Imaging Science Subsystem (ISS) during 4 separate eclipses (eclipses A, B, C, and D) of Io from December 27, 2000 to January 5, 2001. One of these imaging sequences (eclipse A) was mistimed and captured only the start of the eclipse on December 27, 2000. The second sequence (eclipse B) took place on December 29, 2000 from 09:04 to 11:27 UT. The third (eclipse C) imaged from 22:06 UT on January 1, 2001 to 00:28 UT on January 2, 2001. The last sequence (eclipse D) covered the period from 11:03 to 12:44 UT on January 5, 2001. An additional, earlier Io eclipse sequence was also planned but was canceled due to problems with one of the spacecraft reaction wheels. The spatial resolution of these pictures ranged from 60 to 68 km/pixel for the full resolution images and from 120 to 136 km/pixel for summation mode images in which adjacent pixels were summed to increase the signal to noise ratio. Cassini's CCD camera is sensitive to shorter wavelengths than Galileo's and could record more colors using a greater variety of filters. Observations of the first three eclipses were made using 5 colors (CLEAR, UV3, RED + GREEN, CB1, and IR4), while the last eclipse (eclipse D) was imaged using 15 different filter combinations (see Table 1 for a complete list of the filters and bandpasses). Similar views of Io's orbital trailing hemisphere were seen during each eclipse; Cassini's Io-centered longitude shifted only 38 degrees during the week of observations as a result of the spacecraft's motion. However, the eclipses differed greatly from one an-

Table 1
Emission intensity of anti-jovian equatorial glow in eclipse D (January 5, 2001)

Filter name	Center wavelength (nm)	Bandpass (nm)	Emission intensity (kR) or detection limit	Comments
Clear	611	235–1100	336 ± 32	
UV1	258	235–280	< 61	
UV2	298	265–330	56 ± 27	Near detection limit
UV3	338	300–380	149 ± 24	
BL1	451	390–500	102 ± 8	
GRN	568	495–635	41 ± 2	
R + G	601	570–635	12 ± 4	Near detection limit
CB1	619	595–615, 625–645	26 ± 5	
RED	650	570–730	43 ± 3	
HAL	656	650–660	< 7	
R + IR1	702	670–730	< 9	
IR1	752	670–850	20 ± 2	
IR2	862	800–940	< 24	Marginal detection
IR3	930	880–1025	< 44	Marginal detection
IR4	1002	980–1100	< 238	

Listed are the means and standard deviations of up to 7 separate measurements, or detection limits where marginal detections or nondetections were made. These values include (are divided by) correction factors from the latest in-flight calibration.

other with respect to the location of Io in Jupiter's magnetic field (Io's System III magnetic longitude, or λ_{III}).

2. Morphology

The Cassini images covered a broad region around Io, capturing an area more than 17 Io radii from the disk in all directions, but no extended corona was detected beyond one Io radius from the satellite. With exposures ranging from 2 to 12 seconds, the images were optimized for the Pele hot spot (Radebaugh et al., 2003) rather than for faint auroral emissions. Images with exposures lasting several seconds were expected to be noticeably smeared, but in-flight star images acquired via reaction wheels demonstrated (too late for Jupiter planning) that images with much longer exposure times could be unsmeared. All three successfully recorded eclipses (B, C, and D) showed broad similarities in clear-filter emission morphology (Fig. 1). Little if any emission could be seen across the disk on this (upstream) side of Io, in contrast to earlier Galileo images showing distinct disk emission on the downstream side (Geissler et al., 2001). The brightest glows were observed along the equator, near the sub-Jupiter (longitude 0) and anti-Jupiter (longitude 180) points. Little volcanic plume activity could be detected near these locations in the Cassini images, so the equatorial glows were fairly symmetric, uniform and diffuse compared to many of the Galileo observations reported by Geissler et al. (2001).

The anti-jovian and sub-jovian glows appeared equal in intensity, to within measurement error. The brightness ratio depends strongly on the sub-observer longitude: during the early eclipses B and C, Cassini got a better view of the Jupiter-facing side of Io and the sub-jovian glows were far brighter than the anti-jovian glows. Cassini viewed the trailing hemisphere of Io directly (subspacecraft longitude 270) during eclipse D of January 5, 2001, so that both glows could be seen equally well. Measurements were made over two 3×3 pixel boxes centered on the cores of the two equatorial glows (covering areas of 410 km by 410 km) in 6 clear filter images taken while Cassini's subspacecraft longitude varied from 264 to 277 degrees. The antijove/subjove ratios in these images average to 0.994 ± 0.028.

An extended corona could be seen in Cassini RED (570–730 nm) and CB1 (595–615 and 625–645 nm) filter images reaching heights of up to 900 km, or half of Io's radius. Presumably due to neutral atomic oxygen emissions ([OI] 630, 636 nm), these faint equatorial glows track the changing locations of the shorter wavelength equatorial emissions (see next sections) but at greater altitudes above Io's surface.

In addition to the equatorial emissions, a glow encircling Io along the limb could be seen at visible to near-infrared wavelengths from 500 to 850 nm (Cassini GRN to IR1 filters). As in previous Galileo observations (Geissler et al. 1999, 2001), the limb glow appeared brightest on the side of Io that was closest to the plasma torus center. This was particularly evident during eclipse B on December 29, 2000, while Io was below the equatorial plane of the jovian magnetic field at magnetic longitudes from 43 to 106 degrees, and the limb appeared distinctly brighter in the northern hemisphere than in the south.

Sporadic local brightening of the diffuse limb glow near the north pole of Io was seen in all three eclipses, probably caused by a plume erupting from the volcano Tvashtar (63° N, 125° W; on the side of Io opposite to that seen by

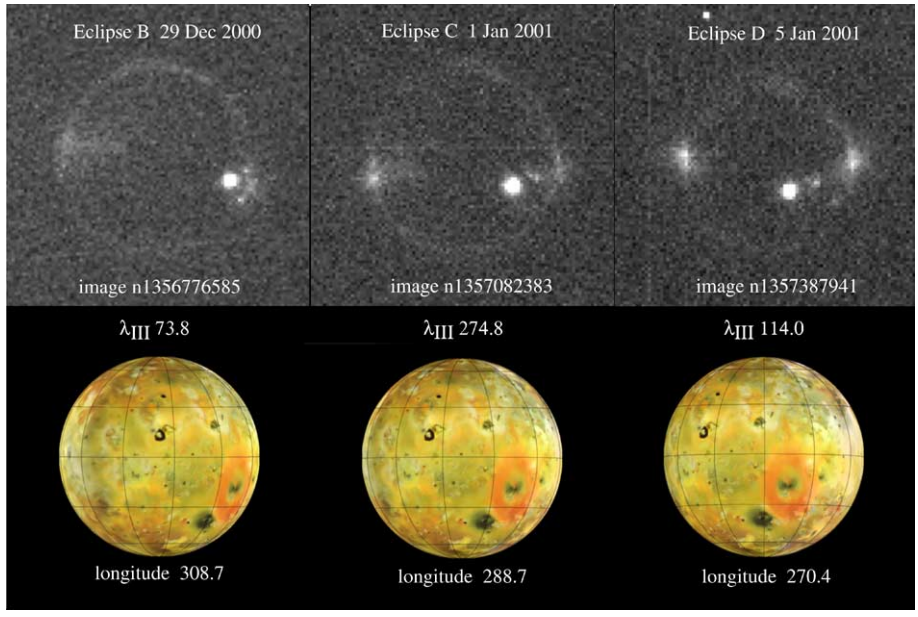

Fig. 1. Comparison of Cassini images from the three successfully recorded eclipses. These clear-filter, full resolution images were acquired near the midpoint of the eclipses and have been cropped to show just the area around the satellite. Galileo images reprojected to similar viewing geometries are shown along the bottom, with latitudes and longitudes marked at 30 degree intervals. The resolution of the Cassini images decreased from 60.5 km/pixel through 61.3 km/pixel to 68.2 km/pixel during the period of observation. The brightest spot shows thermal emission from the volcano Pele.

Cassini) that was later found to have deposited a red ring of sulfur around the volcano more than 1300 km in diameter (McEwen et al., 2001; Porco et al., 2003). Tvashtar caused a knot of emission that could be seen in the near-ultraviolet (Cassini UV3) and blue (BL1) filter images. Tvashtar's plume gases must have reached altitudes of ∼ 380 km to be observed by Cassini extending several pixels over Io's limb.

Local emission associated with volcanic activity could also be seen near the equator on the Jupiter-facing side of Io. A bright band extended eastwards along the equator from the sub-Jupiter point, likely associated with plumes from the volcano Acala and several small volcanic centers in this region detected by Galileo images showing high temperature thermal emission from a cluster of small hot spots (McEwen et al., 1998a). This region is also bright in near-ultraviolet (UV3) images, indicating that Cassini observed non-thermal (atmospheric) emissions.

Thermal emission from several active volcanoes was detected in all of the clear and long-wavelength imaging sequences, particularly at Pele (18° S, 255° W). Hot spots were evident at Reiden (12° S, 234° W) and Wayland Patera (33° S, 223° W), a volcanic center that had never before been detected at visible and near-IR wavelengths. Faint hot spots were also detected at Loki (10° N, 308° W) and at Pillan (11° S, 241° W), the site of an enormous eruption 30 months earlier (McEwen et al., 1998b).

3. Temporal variability

A major advantage of Cassini over previous observations was the capability to record entire eclipses at intervals of minutes (Porco et al., 2003). Animated sequences of images from the best sampled eclipses (B and C) are available on-line at http://www.sciencemag.org/cgi/content/full/299/5612/1541/DC1, Movie S3 (Porco et al., 2003) and http://astrogeology.usgs.gov/Projects/IoAurorae.

Figures 2 and 3 show how Io's clear-filter disk-integrated brightness varied during eclipses B and C. These measurements were taken from raw clear-filter images with the periodic noise removed by frequency domain filtering. Variations in background level were subtracted by averaging the space surrounding Io. This approach has the effect of eliminating possible variations in the extended corona (i.e., extending beyond 17 Io radii) and yields measurements with an arbitrary scale (mean digital number) but avoids the noise introduced by calibration uncertainties. Calibrated images show that the absolute brightness of Io was slightly higher during eclipse C (when Io was near the center of the plasma torus) than during eclipse B (near the edge of the plasma torus, at $\lambda_{III} = 43$ to 106).

We can quantify the post-ingress dimming and pre-egresss brightening of Io by fitting straight lines to the linear portions of the light curves and assign uncertainties to the dimming and brightening times (dashed lines in Figs. 2 and 3) using the standard errors in the y-estimates from the linear regressions. In both cases the disk-averaged emission diminished gradually for the first 17 to 19 minutes after ingress, remained largely steady for the duration of the eclipse, and then began to brighten again ∼ 12 to 13 minutes before egress. This behavior suggests that images acquired within a few minutes of eclipse ingress or egress are contaminated by sunlight scattered into Jupiter's shadow

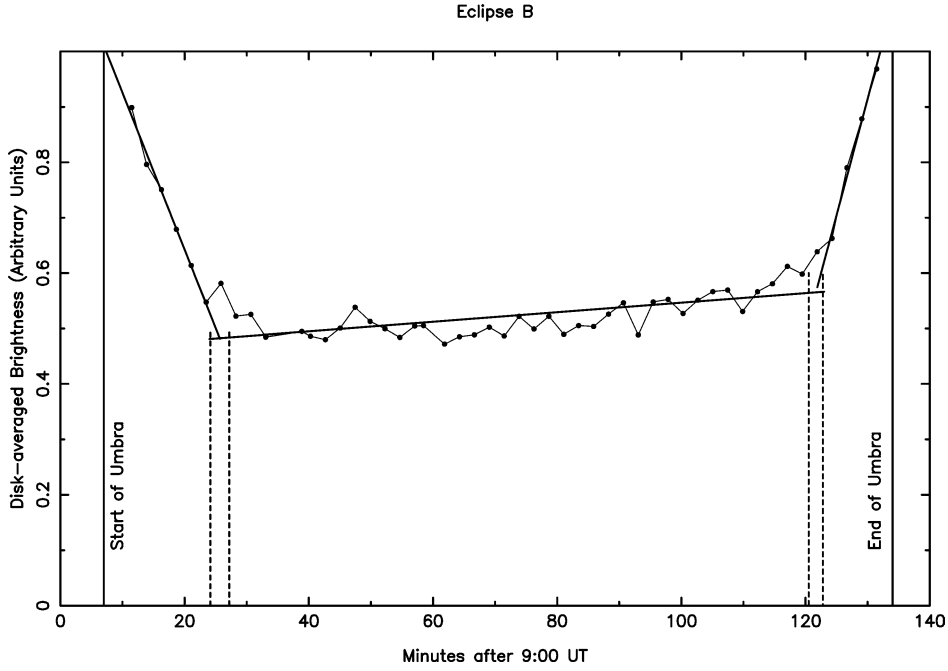

Fig. 2. Time-series of disk-integrated intensities from eclipse B. This figure shows the total brightness of Io as a function of time, from raw Cassini images taken under constant conditions. Solid lines show linear least-squares fits to the data; dashed lines show the formal uncertainty in the times of intersections of the fit lines.

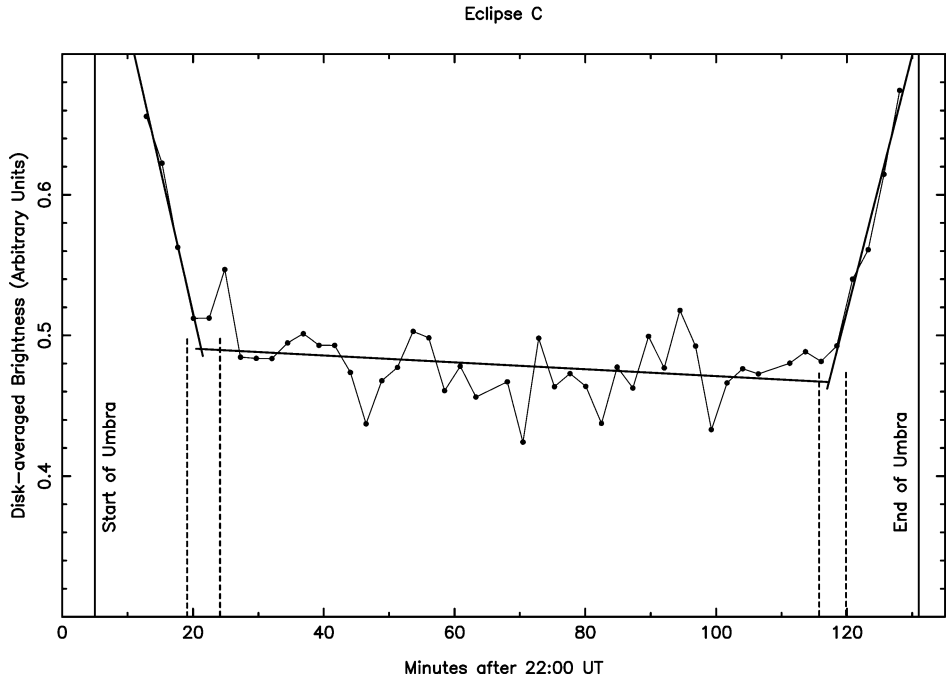

Fig. 3. Time-series of disk-integrated intensities from eclipse C. This figure shows the total brightness of Io as a function of time, from raw Cassini images taken under constant conditions. Solid lines show linear least-squares fits to the data; dashed lines show the formal uncertainty in the times of intersections of the fit lines.

by Rayleigh scattering in the planet's upper atmosphere (cf. Formisano et al., 2003). This is important in that it provides an explanation for the dramatic dimming previously seen in Galileo images at the start of two eclipses (Geissler et al., 1999), because the earlier images in both pairs of Galileo pictures were acquired within 15 minutes of ingress. However, the asymmetry between post-ingress dimming and egress brightening times suggested by Figs. 2 and 3 is consistent with a partial collapse of Io's atmosphere during the first few minutes of eclipse (e.g., Clarke et al., 1994) and constrains the phenomenon to take place within ~ 20 minutes of ingress. Alternatively, the differences between the ingress and egress profiles might be attributable to longitudinal asymmetry in Jupiter's stratospheric haze (West, 1988; Rages et al., 1999).

Io crossed the plasma torus center during eclipse C on January 1, 2001, as it passed through System III magnetic longitudes from 250 to 303 degrees. The equatorial glows were seen to shift in latitude during this eclipse, tracking the tangent points of the jovian magnetic field lines. Figure 4 shows three clear-filter images taken near the start, middle and end of the eclipse, along with the locations of the tangent points of Jupiter's magnetic field lines calculated using the approximate (but adequate) expression: anti-jovian tangent point latitude = Io's magnetic latitude + 9.6 sin(Io's magnetic longitude − 112). Part of the change in Io's appearance was due to the moon's rotation; Cassini's sub-spacecraft longitude started at 281 degrees West and reached 297 degrees West by the end of the sequence. The equatorial glow on the anti-Jupiter side of Io (on the right) could be seen to migrate southwards, while the glow on the Jupiter-facing side (left) shifted towards the north, in accord with the changing orientation of the jovian magnetic field. This behavior is similar to that observed for far-ultraviolet and other atomic emissions (Roesler et al., 1999; Retherford et al., 2000), indicating that these mostly molecular emissions and the atomic emissions are excited by a common population of electrons.

4. Multispectral observations

Five-color imaging at reduced resolution (in summation mode) was also acquired during eclipses B and C. Results from these two imaging sequences were similar. Plate 1a is a false color image from eclipse C made up of three of the five colors: emission in the UV3 filter (300–380 nm) is shown as blue in Plate 1a, while green denotes emission in CB1 (595–645 nm, excluding 615–625 nm) presumably due to neutral atomic oxygen ([OI] 630, 636 nm) emissions. Pele glows brightly due to thermal emission from high-temperature lava in the near-infrared IR4 band (980–1100 nm), displayed as red in Plate 1a, and is also seen more faintly in CB1 as the yellow spot at the center of Pele in Plate 1a. Plate 1b shows two of these colors superimposed on a full resolution clear filter image; emission in the UV3 filter is again shown as blue in Plate 1b, but here the visible CB1 emission (which would appear red to the eye) is shown as red. The blue (UV3) glows correspond to the brightest emissions in the clear filter images and are concentrated near the equator and close to the surface of Io. The red (CB1) emissions are much more extensive, reaching up to 900 km above the moon's surface. This distribution is consistent with their interpretation as molecu-

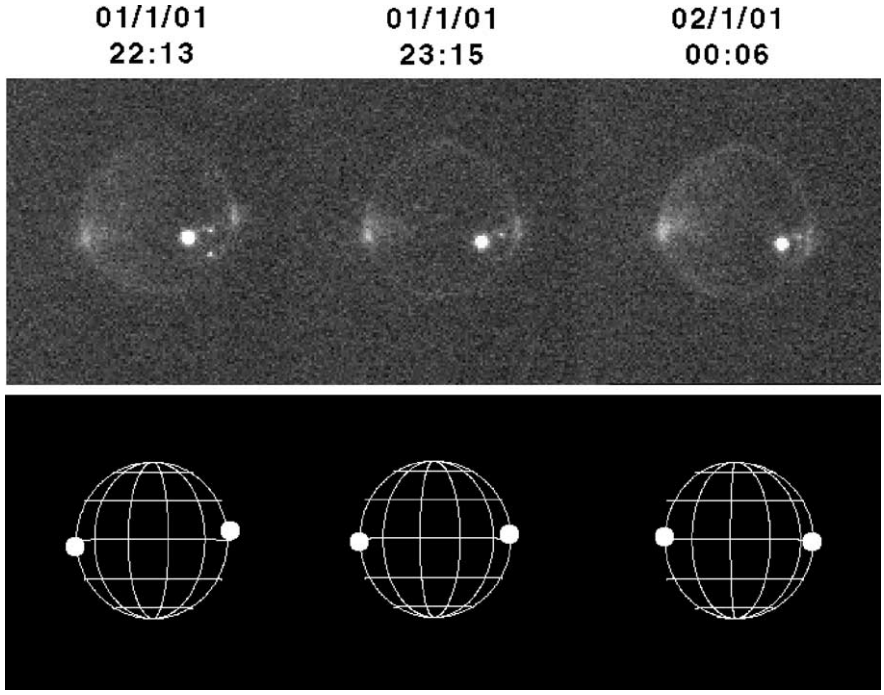

Fig. 4. Time-lapse sequence of clear-filter images of Io during the eclipse of January 1, 2001. Shown for comparison are the approximate locations of the tangent points of the jovian magnetic field lines at the sub-Jupiter and anti-Jupiter points.

lar sulfur dioxide (blue) and atomic oxygen (red) emissions, since the heavier molecule should have a smaller scale height than atomic oxygen. Atomic oxygen is four times lighter than SO_2 and would be expected in Io's thin atmosphere to potentially have a scale height four times larger than SO_2. In addition, the principal source of O atoms during eclipse is electron impact dissociation of SO_2, which is known to produce non-thermal O atoms with characteristic initial random kinetic energy temperature of $E \sim 1$ eV (Vatti Palle et al., 2004), possibly enhancing the scale height for oxygen. Distinct equatorial glows are observed in the oxygen emissions along with limb glows that are brightest near Io's south pole. Other CB1 images from this sequence show that the equatorial oxygen glows follow the motion of the brighter blue (UV3) emissions. A knot of blue emission can also be seen near Io's north pole, presumably due to SO_2 vented from the volcano Tvashtar.

The best spectral measurements of the glows were made during the final eclipse (D) on January 5, 2001, when fifteen different filter combinations were used for long exposure (12 seconds) summation mode imaging (Fig. 5). Table 1 lists the mean measured brightness of the anti-jovian equatorial glow in each bandpass and the upper limits in the cases where no positive detection was made. All of the equatorial glows were measured using a 5×5 pixel box, covering an area of about 680 km $\times$ 680 km in these 2×2 summation mode images. This area is larger than the dimensions of the glows, and the central portions of the glows consistently reach brightness values higher than these averages by a factor of 2 to 3. Hence, the mean value of the brightest 136 km $\times$ 136 km pixel intensity in the clear filter is 752 ± 134 kR. Up to 7 separate measurements were made in each filter combination during eclipse D. The errors reported in Table 1 represent the standard deviations of these individual measurements.

The equatorial glows were detected at visible, near-infrared and near-ultraviolet wavelengths. More than 100 kR were recorded in the ISS UV3 filter (300–380 nm) along with a similar intensity in BL1 (390–500 nm), comparable to Galileo estimates of violet filter intensities (Geissler et al., 1999). At least 50 kR (the detection limit for this filter) were detected in UV2 images (265–330 nm). No detection was made in UV1 (235–280 nm), allowing us to place an upper limit of about 100 kR.

The Cassini detections of near-ultraviolet emissions from the equatorial glows agree with their interpretation as molecular SO_2 emissions, based on laboratory measurements of electron-induced fluorescence of SO_2 (Miller and Becker, 1987; Ajello et al., 1992, 2002). The SO_2 MUV2 band peaks in the near-ultraviolet and extends to visible wavelengths. However, the ratio of BL1/UV3 (i.e., the ratio of intensities in the BL1 and UV3 filters) seems to be larger than expected for SO_2 alone. To verify this, we performed a detailed calculation of the raw signal expected from SO_2 when imaged by Cassini ISS, using the laboratory SO_2 spectrum of Ajello et al. (2002) and the ISS system and filter transmissivities and quantum efficiency as functions of wavelength. The results (Table 2) indicate that the raw DN observed in the BL1 filter is more than three times greater than predicted, relative to the UV3 filter, from laboratory measurements made with electron temperatures in the range 8 to 18 eV (higher electron temperatures appear to be ruled out by the observed

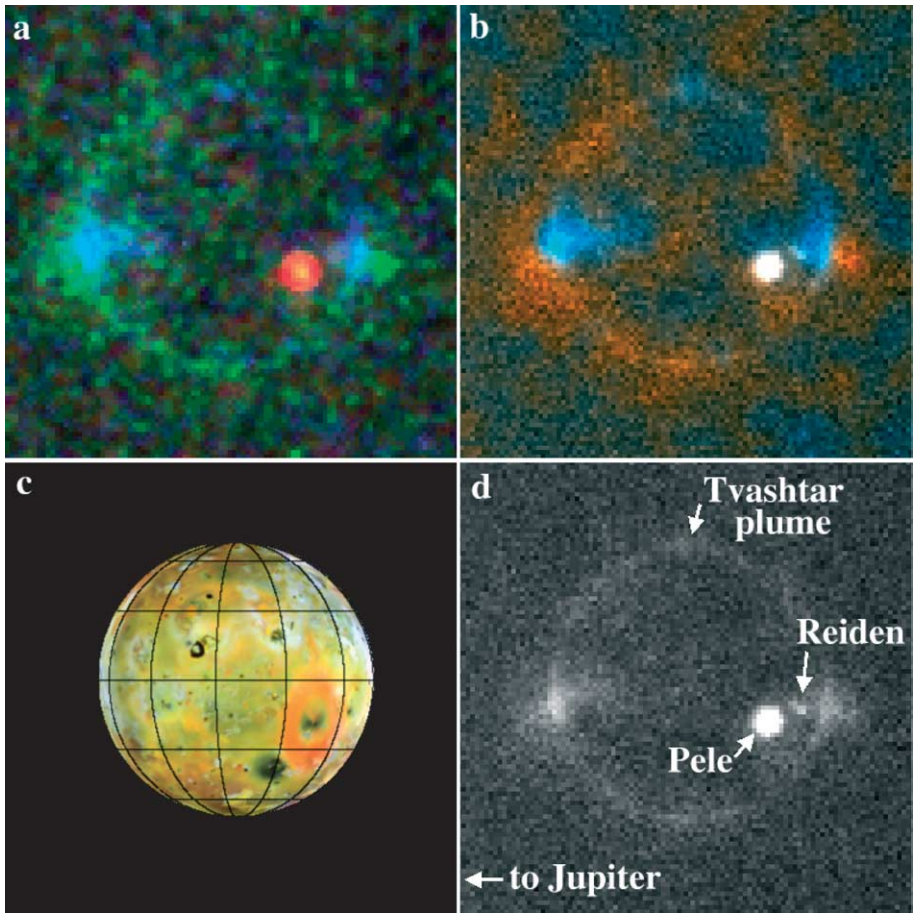

Plate 1. Multispectral images of Io during the eclipse of January 1, 2001. (a) False color composite made up of IR4, CB1, and UV3 images portrayed as red, green and blue, respectively. (b) CB1 (red) and UV3 (blue) images superposed on clear filter image. (c) Location reference map with grid lines at 30 degree intervals. (d) Annotated clear-filter image showing locations of volcanoes and plume glows discussed in text.

Table 2
Raw digital number expected from ISS when imaging SO_2 fluorescence, normalized to unity in the UV3 bandpass

Filter	8 eV	18 eV	98 eV	Measured (DN)
UV1	0.0	0.34	0.36	< 1.0
UV2	0.33	0.42	0.41	0.30 ± 0.04
UV3	1.00	1.00	1.00	1.00 ± 0.11
BL1	0.27	0.39	0.79	0.93 ± 0.13
GRN	0.29	0.20	0.97	0.96 ± 0.14
CLR	3.12	4.30	5.77	5.59 ± 0.70

This table shows the raw signal (DN) expected from an SO_2 source emitting a known number of photons per wavelength increment, using values from the laboratory measurements of Ajello et al. (2002). The predicted ratios take into account the wavelength-dependent sensitivities of the optical and electronic components of ISS and are adjusted (multiplied) using the latest correction factors from in-flight calibration. The measured signals from eclipse D are shown for comparison.

UV2 : UV3 ratio). The GRN filter signal is also elevated, but other constituents such as O and Na are known to contribute to the GRN filter emissions and thus place constraints on the possible amount of SO_2 emission produced by high temperature electrons. The larger-than-expected BL1 intensity requires another emitting species in addition to SO_2 in order to account for the brightness of the equatorial glows between 395 and 500 nm. No line emissions brighter than 0.4 kR were detected by Bouchez et al. (2000) over the wavelength interval between 420 and 500 nm, covering most of the BL1 filter range. The best candidate is the set of $S_2(B^3\Sigma_g^- - X^3\Sigma_u^-)$ bands which span 240–711 nm. For electron energies much above threshold, the most intense S_2 bands are below 350 nm with non-negligible intensity in the BL1 (390–500 nm) filter range. For electron temperatures comparable to threshold excitation energies, the intensity distribution is unknown. Molecular sulfur is a well known volcanically ejected gas and has been spectrally identified in Pele's plume (Spencer et al., 2000).

A clear detection of the equatorial glows was made in the IR1 band (670–850 nm). The equatorial glows were not prominent in either the RED + IR1 filter combination (670–730 nm) or the IR2 filter (800–940 nm), indicating that the emission is mostly in the wavelength range 730 to 800 nm. Atomic potassium (KI 767, 770 nm), sulfur (SI 773 nm), neutral oxygen (OI 777.4, 844.6 nm) and singly ionized oxygen ([OII] 732, 733 nm) are all possible sources of the infrared emission but the largest contribution is likely that of potassium, for reasons explained in the next section.

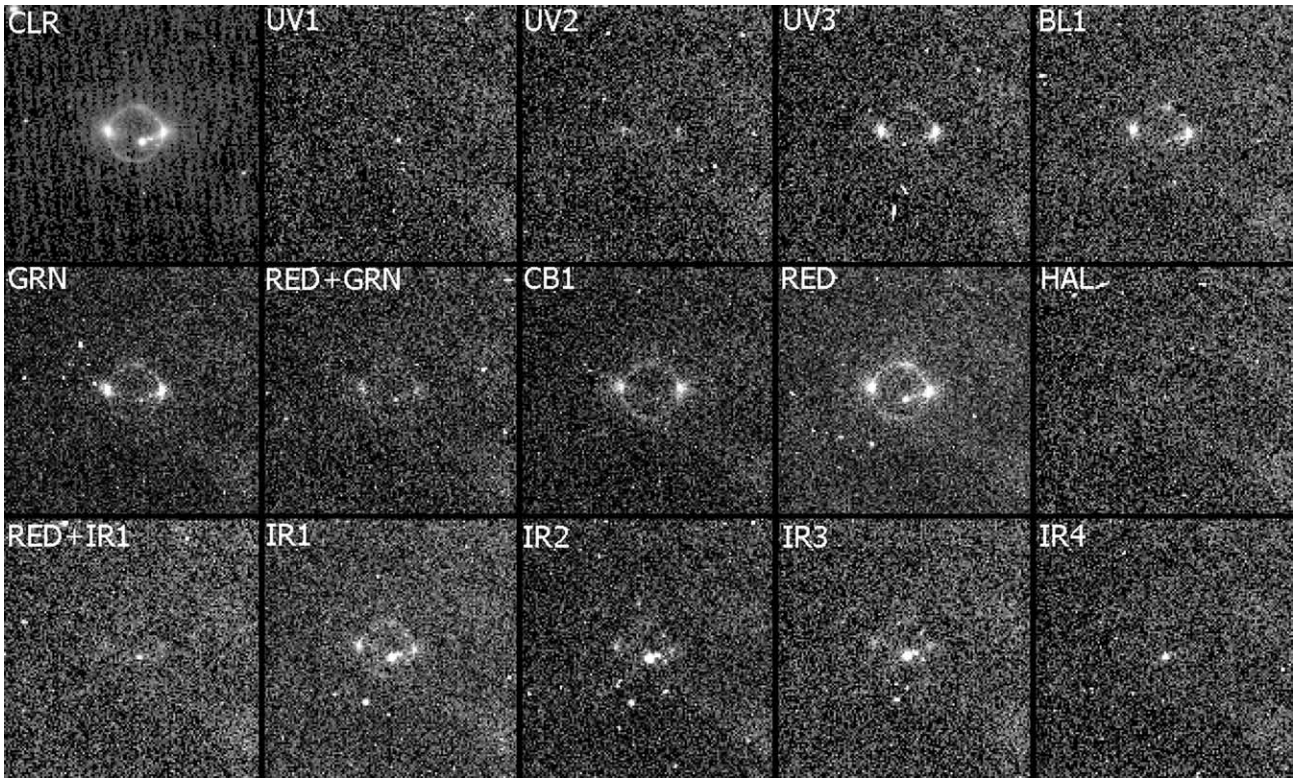

Fig. 5. Montage of spectral images from Eclipse D (January 5, 2001). Equatorial glows were detected at wavelengths from at least 330 nm to 880 nm and in all filters except UV1, HAL and IR4. Limb glows were detected in GRN, CB1, RED, and IR1 filter images.

Table 3
Emission intensity of limb glows in eclipse D (January 5, 2001)

Filter name	Center wavelength (nm)	Bandpass (nm)	Emission intensity (kR)	Comments
Clear	611	235–1100	102 ± 22	N. Pole (including Tvashtar)
Clear	611	235–1100	46 ± 11	S. Pole
GRN	568	495–635	18 ± 7	N. Pole
CB1	619	595–615, 625–645	10 ± 3	N. Pole
RED	650	570–730	23 ± 7	N. Pole
IR1	752	670–850	12 ± 3	N. Pole

Listed are the means and standard deviations of up to 7 separate measurements. These values include (are divided by) correction factors from the latest in-flight calibration.

Marginal detections of the equatorial glows in the IR2 (800–940 nm) and IR3 (880–1025 nm) bands might be explained by OI 845 and 926 nm emissions.

Limb glows distinct from the equatorial emissions were detected in the clear filter images and also in GRN, CB1, RED, and IR1. Brightness measurements were made near the poles of Io using a rectangular 9×3 pixel box with the long axis parallel to the equator, spanning approximately 1220 km, and the short axis in the direction of the pole ($\sim$ 410 km wide). These measurements are listed in Table 3. Although the north polar limb was affected by the eruption of Tvashtar, limb emissions that completely encircled Io were seen in each of the CLR, GRN, CB1, RED, and IR1 filter images from eclipse D (Fig. 5). The specific emissions responsible for the limb glows are presumed to be NaI 589, 590 nm and [OI] 557 nm in the GRN filter; [OI] 630, 636 nm in the CB1 and RED filters; and KI 767, 770 nm in IR1. To our knowledge, these are the first detections of K along Io's limb.

Finally, disk-integrated measurements of the total power radiated by the atmospheric emissions are shown in Table 4. These measurements were made from images edited to remove the thermal emissions from volcanoes Pele and Reiden. Table 4 indicates that much of the power radiated by Io's aurorae was at ultraviolet and short visible wavelengths. For this reason, it is unsurprising that the Cassini ISS estimate of Io's disk-integrated power (3600 MW) is larger than the estimate from Galileo SSI ($\sim$ 2000 MW; Geissler et al., 1999), which was insensitive to UV wavelengths shorter than 390 nm. Because radiated powers were computed assuming that the photons had wavelengths at the center of the bandpasses, the mean Clear filter power of 3600 MW is probably a slight underestimate. Another reason why the power estimated from the Clear filter need not match the sum

Table 4
Disk-integrated measurements of Io's auroral emissions during eclipse D (January 5, 2001)

Filter name	Center wavelength (nm)	Bandpass (nm)	Radiated photons	Radiated power (W)
Clear	611	235–1100	1.24 ± 0.07e+28	3.59 ± 0.22e+09
UV3	338	300–380	3.04 ± 0.68e+27	1.76 ± 0.39e+09
BL1	451	390–500	2.66 ± 1.07e+27	1.17 ± 0.47e+09
GRN	568	495–635	1.54 ± 0.74e+27	0.54 ± 0.26e+09
R + G	601	570–635	0.38 ± 0.48e+27	0.13 ± 0.16e+09
CB1	619	595–615, 625–645	1.16 ± 0.44e+27	0.37 ± 0.14e+09
RED	650	570–730	2.01 ± 0.07e+27	0.62 ± 0.02e+09
IR1	752	670–850	1.11 ± 0.35e+27	0.29 ± 0.10e+09

Photon counts were measured over square boxes that extended an Io diameter away from the disk in all directions, and assume that emission was uniform over 4 pi steradians. Powers were computed assuming that the emissions were at the center wavelengths of each filter. Thermal emission from volcanoes was excluded.

of the individual filter power values is that several of these filter combinations overlap in wavelength.

5. Interpretation

To interpret the Cassini observations we use the model of Saur et al. (1999, 2002) to describe the electrodynamic interaction between Io and the plasma torus. This model explicitly calculates the electron number density N_e and temperature T_e as functions of location in Io's atmosphere, given the values of these quantities in the plasma torus upstream of Io. Details of the model and the physics of these interactions were described by Saur et al. (2003). Here we outline the results of these calculations for the simplified case of a spherically symmetric atmosphere with optically thin emissions, and point out the implications for the column abundances and mixing ratios of Io's atmospheric constituents based on comparisons with the Cassini data.

The intensities of Io's near-ultraviolet emissions place significant constraints on the column abundance of SO_2, as explained by Saur et al. (2000). If the atmosphere is too thin, the torus electrons simply pass through the atmosphere and deposit their energy onto the surface. As the atmosphere gets thicker, the electrodynamic interaction is strengthened and more of the torus electrons are diverted around Io so that fewer deposit their energy into Io's atmosphere. Assuming upstream torus electrons with density $N_e = 3600$ cm^{-3} and temperature $T_e = 5$ eV, Saur et al. (2003) find that the maximum intensity expected from the near-ultraviolet MUV2 bands of SO_2 is attained for column abundances in the range $(0.54–1.7) \times 10^{15}$ cm^{-2}.

Comparison of the Cassini ISS measurements with the Saur et al. (1999) model is not straightforward. The SO_2 atmosphere of Io has a scale height at the surface of ~ 10 and ~ 200 km at its exobase. If we adopt the inferred model atmosphere given in Strobel and Wolven (2001), an ISS pixel tangent to the surface includes the first five scale heights of the atmosphere. The Saur et al. (1999) model has an assumed scale height of 100 km in order to resolve each scale height with three grid points, i.e., with resolution $R_{Io}/50 = 36$ km. Thus the first five scale heights of our model map into the pixel tangent to the surface. On a global basis our model predicts 2×10^{27} photons/s from the SO_2 MUV2 bands when the electron heat conduction flux is handled as described in Appendix A of Saur et al. (2002), in comparison to the ISS measured value of 4.9×10^{27} photons/s. Hence it would appear that our assumed upstream torus electron density and temperature boundary conditions are insufficient to power the observed Io visible aurora. As a check, the analytic solution given in Appendix B of Saur et al. (2003), which does not depend on any particular model for the 3D interaction of torus and atmosphere, is used to calculate the maximum radiation rate if all available power in the torus could be utilized. The result is 3.8×10^{27} photons/s and 80% of the measured value. The difference between the analytic and the 3D model results is the heat conduction time (infinitesimal in the former and finite, but too long, in the latter). Our 3D model results could be brought into better agreement with a shorter heat conduction time constant. In addition, the torus flux tubes may contain more energy than assumed in our model where the electrons are assumed Maxwellian at 5 eV. If the electron distribution function were assumed to be a kappa-distribution, as inferred by Meyer-Vernet et al. (1995) from Ulysses data, then actual energy content could increase by $\sim 50\%$. A time variable flux of field aligned non-thermal electrons (~ 30 eV) were occasionally detected by the Galileo PLS (Frank and Patterson, 1999, 2002) that would also add to the energy content.

Measured equatorial glows averaged over a 5×5 pixel box and covering an area of about 680 km $\times$ 680 km are compared with peak model intensities on the limb in our analysis given below. These intensities are comparable in absolute magnitude and accurate on a relative basis for intercomparison of ratios of filter intensities. Model intensities integrated over Io's disk and atmosphere can be increased to the observed values by depleting the torus energy content faster via a shorter heat conduction time constant.

Partitioning the observed intensities according to the electron impact excitation cross-sections measured at 8 eV by Ajello et al. (2002) for SO_2 yields intensities of 78 kR for the UV2 filter, 125 kR for UV3, 29 kR for BL1, and 10 kR for GRN for a total intensity of 242 kR and within our theoretical range of 180–350 kR. The excess intensities seen

by Cassini must be contributed by other atmospheric constituents, such as O, S, S_2, Na or K.

Two sources of information help to constrain our interpretations. The first is that some of these gases have been observed in Io's atmosphere at far-ultraviolet wavelengths, such as HST/STIS observations of neutral O (135.6 nm) and S (190.0 nm) (Roesler et al., 1999). The abundances inferred from the Cassini observations ought to be consistent with those existing measurements, allowing for variability of Io's atmosphere with time. The second constraint comes from the abundance ratios determined for optically active gases, such as the alkali metals Na and K, that are visible even though they are present in small quantities.

Electron impact on atomic oxygen contributes to the RED, CB1 and GRN filters via the red lines of OI(^{1}D → ^{3}P) at 630.0 and 636.4 nm and the green line OI(^{1}S → ^{1}D) at 557.7 nm, as does electron impact on SO_2. The electron impact excitation cross-sections for O(^{1}S) and O(^{1}D) are based on the laboratory measurements of Doering and Gulcicek (1989a) and Doering (1992). The OI 844.6 nm and OI 777.4 nm multiplets result from cascades and contribute to the IR1 Filter intensities. For OI 135.6 nm, the direct excitation cross-section for ^{5}S term has been measured in the laboratory and our adopted cross-section is based principally on Doering and Gulcicek (1989b). For cascade contributions the review article by Laher and Gilmore (1990) in conjunction with Julienne and Davis (1976) were used to construct the total emission cross-section. Cross-sections for sulfur were computed from the theoretical electron impact collision strengths calculated by Zatsarinny and Tayal (2002). Electron impact of SI into the ^{1}S and ^{1}D terms is followed by ^{1}S → ^{1}D radiative decay to produce the SI 772.5 nm line with probability 0.84 and then ^{1}D → ^{3}P to radiate the SI 1082.0, 1130.6 nm lines in the ratios of 0.77 and 0.23. Prominently contributing to the GRN filter intensity are the NaI D lines at 589.0, 589.6 nm, whereas KI D lines at 766.5, 769.9 nm probably dominate the IR1 filter intensity because the cross-section of K is much higher than other candidate emitters. Electron impact cross-sections for these species were adopted from Kim (2001). These cross-sections are exceedingly large, with peak values of (4–6) × 10^{-15} cm^2 at 6–8 eV. These allowed transitions have large oscillator strengths, so that small column densities yield large intensities. Hence, optical depth effects can be important even at low abundances.

The available data on the electron excitation cross-sections and spectroscopy of S_2 is less than satisfactory. To the authors knowledge no quantitative laboratory measurements have been made for electron excitation of the S_2 B state; only the theoretical electron excitation cross-sections of Garrett et al. (1985) are available. According to Garrett et al., electron impact on S_2 in low vibrational levels leads primarily to bound state excitation of the B $^3\Sigma_g^-$ state rather than dissociation via this state. The latter outcome occurs preferentially by electron impact on isoelectronic O_2 ($v'' = 0$). Their method of calculation does not yield the fraction of predissociation after excitation to bound states. Consequently, the following approximations and assumptions were made. The S_2 is presumed to be vibrationally hot in the atmosphere (> 1000 K) consistent with the high temperatures in the conduits of volcanic vents and the slow vibrational relaxation in Io's thin atmosphere. Excitation from ground state vibrational levels to B state vibrational levels is assumed to be proportional to the Franck–Condon factors given in Anderson et al. (1979). Radiative decay from specific B state vibrational levels to various ground state vibrational levels was computed with theoretical Einstein "A" coefficients supplied by S.R. Langhoff (unpublished and private communication, 2003). These coefficients and the associated Franck–Condon factors are in good agreement with the Anderson et al. (1979) experimentally inferred Franck–Condon factors. As a check, these coefficients also compared favorably with the Einstein A-values adopted by Kim et al. (1990). The calculated Langhoff spectroscopic quantities have the advantage of being more comprehensive (v', $v'' = 0, 1, \ldots, 39$) and self-consistent.

The resultant distributions of S_2 band emission which originate from the first three ground state vibrational levels $v'' = 0, 1, 2$ were partitioned into the relevant ISS filters (UV2, UV3, BL1). For our desired level of accuracy, the intensity ratio of S_2 emission for BL1 : UV3 : UV2 is $1 : 2.3 : \sim 2.3$ for each v'' $(0, 1, 2)$. The observed intensity ratio for BL1 : UV3 is 1 : 1.5. Electron impact emission of SO_2 at low T_e (8–18 eV) yields an intensity ratio for BL1 : UV3 of 1 : 4.3. Thus it is clear that no combination of S_2 and SO_2 band emission can explain the observed filter intensity ratio. If our assumptions are correct, one is forced to invoke some additional emitter(s) to account for the "excess" emission observed in the BL1 filter. Alternatively, one might argue that excitation electrons are hot (∼ 100 eV), but then the inferred intensity ratios would be $0.44 : 1 : 1.64 : 1.36$ for GRN : BL1 : UV3 : UV2 filters, in disagreement with the observed intensities. In particular, when normalized to the BL1 filter, the GRN filter would be all SO_2 emission and the implied SO_2 emission in the UV2 filter would exceed the observed intensity by a factor of 2. Absorption in the UV2 range is unlikely to be important in Io's tenuous atmosphere: SO_2 absorption is at most 10^{-18} cm^{-2} at the inferred column density of $< 2 \times 10^{15}$ cm^{-2}. A more plausible scenario is that excitation of the S_2 B state vibrational levels at threshold electron energies is not proportional to the Franck–Condon factors and lower vibrational levels of the B state have higher probability. Until laboratory data are available, accurate estimates of the partitioning of S_2 band emission cannot be made.

To estimate the S_2 mixing ratio, S_2 is assumed to be solely in the ground state vibrational levels $v'' = 0, 1, 2$ in thermodynamic equilibrium at 1500 K. The electron impact excitation cross-section is taken from Garrett et al. (1985) and adjusted for bound B state predissociation. To achieve 70 kR in the BL1 filter would require a 27% mixing ratio for S_2. If all the S_2 band emission occurred solely in the

Table 5
Calculated intensities for the anti-jovian equatorial spot compared with observed intensities

Filter	Emitters	Mixing ratio (%)	Cross-section peak (10^{-18} cm^2) @ (eV)	Calculated intensity (kR)	Observed intensity (kR)
UV2	SO_2 MUV2	82	16.5 @ 10	64	
	S_2	~ 10, (5–27)	290 @ 10	< 165, cf. text	
	Total			64–229	56 ± 27
UV3	SO_2 MUV2	82	16.5 @ 10	102	
	S_2	~ 10, (5–27)	290 @ 10	< 165, cf. text	
	Total			102–287	149 ± 24
BL1	SO_2 MUV2	82	16.5 @ 10	24	
	S_2	~ 10, (5–27)	290 @ 10	~ 70, cf. text	
	Total			~ 94	102 ± 8
GRN	SO_2 MUV2	82		8	
	OI 557.7	5	3.3 @ 9.5	2.5	
	NaI 589.0	0.12	3830 @ 8	30	
	Total			40.5	41 ± 2
CB1	OI 630, 636.4	5	54 @ 6	31	26 ± 5
RED	OI 630, 636.4	5	54 @ 6	31	43 ± 3
IR1	OI 777.4	5	5.1 @ 20	0.9	
	OI 844.6	5	10 @ 20	1.5	
	SI 772.5	2.5	6.5 @ 11	2.3	
	KI 767	0.036	6170 @ 6	18	
	Total			23	20 ± 2

The chosen mixing ratios imply FUV intensities for OI 135.6 nm: $5 \times 0.32 = 1.6$ kR; and for SI 190 nm: $2.5 \times 1.7 = 4.2$ kR.

BL1 filter at 70 kR, then the required S_2 mixing ratio would decrease to 5%. Within this mixing ratio range (5–27%), a representative value of ~ 10% would be most reasonable in light of all the assumptions and uncertainties. This mixing ratio range is comparable to what Spencer et al. (2000) inferred for the Pele plume.

Table 5 shows our best-fit predictions of Io's auroral equatorial emission intensities compared with the intensities measured in the anti-Jupiter equatorial bright spot. It should be noted that we have no spectral features to infer the SO mixing ratio, which is on the order of a few percent (Lellouch et al., 1996). We assume an O mixing ratio of 5% to match the CB1 filter, a S mixing ratio of 2.5% (which gives SI 190 nm in the range seen by HST), a S_2 mixing ratio of ~ 10% to match the residual of observed BL1 filter intensity minus SO_2 MUV2 band intensity, a Na mixing ratio of 3.3×10^{-4} to match the residual in the GRN filter, and a K mixing ratio of 1.2×10^{-4} to match the bulk of the IR1 filter, under the assumption that these resonance lines are optically thin. A quick check at these very low mixing ratios indicates that these lines have total tangential optical depths in the range of 4–12. The method of Gladstone (1985) is used to treat approximately the radiative transfer of these resonance lines generated by the internal source of electron impact excitation. Io's atmosphere can be treated at these visible wavelengths as a pure scattering atmosphere with single-scattering albedo, $\omega_0 = 1$. The finite scattering optical depth atmosphere with an internal electron impact excitation source of Na and K D lines requires an enhancement of the inferred Na and K mixing ratios over values derived from optically thin intensities by factors of 3.5 and 3, for Na and K, respectively. Thus the Na mixing ratio is $\sim 1.2 \times 10^{-3}$ and the K mixing ratio is $\sim 3.6 \times 10^{-4}$. The implied Na/K ratio is ~ 3.3, which is a factor of 2–3 below the quoted range in Brown (2001) of $\sim 10 \pm 3$. However, if the SO_2 contribution to the GRN filter were much lower, then a Na mixing ratio of 1.8×10^{-3} would be needed to match the GRN filter and the Na/K ratio would be 5. Also, the photoionization lifetime of K is ~ 20% shorter than the Na photoionization lifetime, which implies the atmospheric Na/K must be lower than the coronal Na/K derived by Brown (2001). Hence our inferred Na/K ratio is consistent with the Brown (2001) value.

One complication is that O(^{1}D) reacts or is quenched rapidly by most molecules with a rate of $(0.4–2) \times 10^{-10}$ cm^3/s, in competition with its radiative decay rate of 0.00681 s^{-1}. While this quenching rate has not been measured for SO_2, a reasonable estimate is 1×10^{-10} cm^3/s. Thus quenching and radiative decay are equally probable when the SO_2 number density is 6.8×10^7 cm^{-3}. Hence OI red line emissions do not originate near the surface, but are confined to elevated levels within three scale heights of the exobase in the equatorial atmosphere of Strobel and Wolven (2001).

6. Discussion

The Cassini observations strengthen the case that the bright blue equatorial glows seen in the Galileo pictures are the visible tails of molecular SO_2 emissions that peak

at near-ultraviolet wavelengths. These broadband molecular emissions are difficult to detect from Earth, owing to the scattered light from nearby Jupiter. The new observations also show that the molecular emissions move about Io, following the magnetic field of Jupiter. Like their counterparts caused by atomic emissions, the SO_2 glows appear to be powered by electrodynamic interactions between Io and the plasma torus, controlling the electron energy flow patterns into Io's atmosphere (Saur et al., 2000).

Cassini monitored Io's appearance over entire eclipses, documenting temporal changes on time scales of minutes. These data provide an explanation for the dramatic changes seen by Galileo during the first few minutes after ingress and help constrain the degree of atmospheric collapse when Io enters Jupiter's shadow. The contribution of light scattered into Jupiter's shadow by aerosols or gases in the jovian atmosphere is demonstrated by the pre-egress brightening observed on Io by Cassini, beginning some 12 to 13 minutes prior to the satellite exiting the planet's umbra. Post-ingress dimming takes substantially longer, suggesting that partial collapse of the sublimation-driven atmosphere does indeed take place (assuming that Jupiter's stratospheric aerosols were similar on the dusk and dawn limbs). However, the persistence of auroral glows and the column densities inferred from modeling their intensities indicate that a significant component of Io's atmosphere is retained in the absence of sunlight, presumably supported by volcanism.

Detailed comparisons of the equatorial glow intensities with the spectrum of electron-induced fluorescence of SO_2 suggest that the equatorial glows are produced by a combination of gases including SO_2, O, S_2, Na, and K. The sources of the potassium and sodium in Io's torus are of great interest from a geological point of view, given the recent identification of Cl in the torus with abundances that suggest that the metals may have derived from salts (Schneider et al. , 2000) and the recent detection of gaseous NaCl in volcanic plumes by Lellouch et al. (2003). The Cassini results are consistent with Na and K derived from primary volcanic gases of NaCl and KCl (Fegley and Zolotov, 2000). In particular, the inferred $NaCl/SO_2$ flux ratios for volcanic models are in the range of $(0.4–13) \times 10^{-3}$ with the smaller values appropriate for co-location with SO_2 and the larger values appropriate for preferential concentration near volcanic vents. It should also be noted that the inferred Na tangential column density at peak emission, $\sim (1.2–1.8) \times 10^{12}$ cm^{-2}, is comparable to the Na column density of 1.1×10^{12} cm^{-2} derived by Schneider et al. (1991) at 1.4 Io radii.

7. Conclusions

The above analyses lead to the following conclusions concerning Io's visible aurorae:

(1) Detection of the bright equatorial glows in Cassini's near-ultraviolet (UV2 and UV3) filters supports the interpretation that the emissions are due to molecular SO_2. The visible glows likely represent the long-wavelength tails of the MUV2 emissions identified from laboratory measurements of electron-induced SO_2 fluorescence.

(2) Detailed comparisons of laboratory SO_2 spectra with the Cassini observations indicate that a mixture of gases make up the equatorial emissions. Potassium is suggested by new detections of the equatorial glows at near-infrared wavelengths from 730 to 800 nm. Neutral atomic oxygen and sodium are required to explain the brightness of the glows at visible wavelengths. The best candidate for the excess intensity of the glows in the BL1 filter wavelength interval (390–500 nm) is S_2 ($B\,^3\Sigma_g^- – X\,^3\Sigma_u^-$).

(3) Stratification of the atmosphere is demonstrated by differences in the altitudes of emissions at various wavelengths. The near-ultraviolet (SO_2) emissions are confined to a region close to Io's surface, whereas neutral oxygen emissions are seen at altitudes that reach up to 900 km, or half the radius of the satellite.

(4) The locations of both the molecular (SO_2) and atomic (O) visible emissions vary in response to the changing orientation of the external magnetic field, tracking the tangent points of the jovian magnetic field lines. This behavior of the visible aurorae had not previously been observed directly or simultaneously, but was inferred from analysis of a collection of Galileo observations acquired with a variety of viewing geometries.

(5) Limb glows distinct from the equatorial emissions were observed at visible to near-infrared wavelengths from 500 to 850 nm. The limb glows, brighter on the side of Io closest to the center of the plasma torus, indicate that O, Na, and K are distributed across Io's surface and not simply confined to the equatorial regions.

(6) Pre-egress brightening demonstrates that light scattered into Jupiter's shadow by gases and aerosols in the giant planet's upper atmosphere contaminates images of Io taken within 13 minutes of entry into or emergence from Jupiter's umbra. Although partial atmospheric collapse is suggested by the longer timescale for post-ingress dimming than pre-egress brightening, Io's atmosphere must be substantially supported by volcanism to retain auroral emissions throughout the duration of eclipse.

Acknowledgments

We thank Kurt Retherford for helpful discussions and two careful referees for constructive comments. D.F.S. thank Stephanie R. Langhoff for supplying her unpublished calculations of S_2 Franck–Condon factors and Einstein *A* coefficients for this research. D.F.S. and J.S. were supported by JPL Cassini Mission Contract No. 961155 and NASA grants NAG5-4168 and 12051. C.P. and A.S.M. were supported by the Cassini project.

References

Ajello, J.M., James, G.K., Kanik, I., 1992. The complete UV spectrum of SO_2 and electron impact. II. The middle ultraviolet spectrum. J. Geophys. Res. 97, 10501–10512.

Ajello, J.M., Hansen, D.L., Beegle, L.W., Terrell, C.A., Kanik, I., James, G.K., Makarov, O.P., 2002. The middle ultraviolet and visible spectrum of SO_2 by electron impact. J. Geophys. Res. 107. 10.1029, 2.1–2.7.

Anderson, W.R., Crosley, D.R., Allen, J.E., 1979. Franck–Condon factors for the B–X system of S_2. J. Chem. Phys. 71, 821–829.

Belton, M.J.S., Head, J.W., Ingersoll, A.P., Greeley, R., McEwen, A.S., Klaasen, K.P., Senske, D., Pappalardo, R., Collins, G., Vasavada, A.R., Sullivan, R., Simonelli, D., Geissler, P., Carr, M.H., Davies, M.E., Veverka, J., Gierasch, P.J., Banfield, D., Bell, M., Chapman, C.R., Anger, C., Greenberg, R., Neukum, G., Pilcher, C.B., Beebe, R.F., Burns, J.A., Fanale, F., Ip, W., Johnson, T.V., Morrison, D., Moore, J., Orton, G.S., Thomas, P., West, R.A., 1996. Galileo's first images of Jupiter and the galilean satellites. Science 274, 377–385.

Brown, M.E., 2001. Potassium in Europa's atmosphere. Icarus 151, 190–195.

Bouchez, A.H., Brown, M.E., Schneider, N.M., 2000. Eclipse spectroscopy of Io's atmosphere. Icarus 148, 316–319.

Clarke, J.T., Ajello, J., Luhmann, J., Schneider, N., Kanik, I., 1994. Hubble Space Telescope UV spectral observations of Io passing into eclipse. J. Geophys. Res. 99, 8387–8402.

Cook, A.F., Shoemaker, E.M., Smith, B.A., Danielson, G.E., Johnson, T.V., Synnott, S.P., 1981. Volcanic origin of the eruptive plumes on Io. Science 211, 1419–1422.

Doering, J.P., 1992. Absolute differential and integral electron excitation cross sections for atomic oxygen. 9. Improved cross section for the ^3P–^1D transition from 4.0 to 30 eV. J. Geophys. Res. 97, 19531–19534.

Doering, J.P., Gulcicek, E.E., 1989a. Absolute differential and integral electron excitation cross sections for atomic oxygen. 7. The ^3P–^1D and ^3P–^1S transition from 4.0 to 30 eV. J. Geophys. Res. 94, 1541–1546.

Doering, J.P., Gulcicek, E.E., 1989b. Absolute differential and integral electron excitation cross sections for atomic oxygen. 8. The ^3P–$^5S^0$ transitions (1356A) from 13.9 to 30 eV. J. Geophys. Res. 94, 2733–2736.

Fegley Jr., B., Zolotov, M.Y., 2000. Chemistry of sodium, potassium, and chlorine in volcanic gases on Io. Icarus 148, 193–210.

Formisano, V., D'Aversa, E., Bellucci, G., Baines, K.H., Bibring, J.P., Brown, R.H., Buratti, B.J., Capaccioni, F., Cerroni, P., Clark, R.N., 17 colleagues, 2003. Cassini-VIMS at Jupiter: solar occultation measurements using Io. Icarus 166, 75–84.

Frank, L.A., Paterson, W.R., 1999. Intense electron beams observed at Io with the Galileo spacecraft. J. Geophys. Res. 104, 28657–28669.

Frank, L.A., Paterson, W.R., 2002. Galileo observations of electron beams and thermal ions in Jupiters' magnetosphere and their relationship to the auroras. J. Geophys. Res. 107 (A12). 1478, 35-1–35-17.

Garrett, B.C., Redmon, L.T., McCurdy, C.W., Redmon, M.J., 1985. Electronic excitation and dissociation of O_2 and S_2 by electron impact. Phys. Rev. A 32, 3366–3375.

Geissler, P.E., McEwen, A.S., Ip, W., Belton, M.J.S., Johnson, T.V., Smyth, W.H., Ingersoll, A.P., 1999. Galileo imaging of atmospheric emissions from Io. Science 285, 870–874.

Geissler, P.E., Smyth, W.H., McEwen, A.S., Ip, W., Belton, M.J.S., Johnson, T.V., Ingersoll, A.P., Rages, K., Hubbard, W., Dessler, A.J., 2001. Morphology and time variability of Io's visible aurora. J. Geophys. Res. 106, 26137–26146.

Gladstone, G.R., 1985. Radiative transfer of resonance lines with internal sources. J. Quant. Spectrosc. Radiat. Transfer 33, 453–458.

Julienne, P.S., Davis, J., 1976. Cascade and radiation trapping effects on atmospheric atomic oxygen emission excited by electron impact. J. Geophys. Res. 81, 1397–1403.

Kim, Y.-K., 2001. Scaling of plane-wave Born cross sections for electron-impact excitation of neutral atoms. Phys. Rev. A 64, 032713–032722.

Kim, S.J., A'Hearn, M.F., Larson, S.M., 1990. Multi-cycle fluorescence: application to S_2 in Comet IRAS–Araki–Alcock 1983VII. Icarus 87, 440–451.

Laher, R.R., Gilmore, F.R., 1990. Updated excitation and ionization cross sections for electron impact on atomic oxygen. J. Phys. Chem. Ref. Data 19, 277–305.

Lellouch, E., Strobel, D.F., Belton, M.J.S., Summers, M.E., Paubert, G., Moreno, R., 1996. Detection of sulfur monoxide in Io's atmosphere. Astrophys. J. Lett. 459, L107–L110.

Lellouch, E., Paubert, G., Moses, J.I., Schneider, N.M., Strobel, D.F., 2003. Volcanically-emitted sodium chloride as a source for Io's neutral clouds and plasma torus. Nature 421, 45–47.

McEwen, A.S., Keszthelyi, L., Geissler, P.E., Simonelli, D.P., Carr, M.H., Johnson, T.V., Klaasen, K.P., Breneman, H.H., Jones, T.J., Kaufman, J.P., Magee, K.P., Senske, D.A., Belton, M.J.S., Schubert, G., 1998a. Active volcanism on Io as seen by Galileo SSI. Icarus 135, 181–219.

McEwen, A.S., Keszthelyi, L., Spencer, J.R., Schubert, G., Matson, D.L., Lopes-Gautier, R., Klaasen, K.P., Johnson, T.V., Head, J.W., Geissler, P.E., Fagents, S., Davies, A.G., Carr, M.H., Breneman, H.H., Belton, M.J.S., 1998b. High-temperature silicate volcanism on Jupiter's moon Io. Science 281, 87–90.

McEwen, A., Geissler, P., Belton, M., Porco, C., Pappalardo, R., Johnson, T., Squyres, S., Williams, D., Head, J., 2001. Cassini and Galileo satellite imaging results; giant north polar plume on Io. In: American Geophysical Union, Spring Meeting 2001. Abstract #P51A-04.

Meyer-Vernet, N., Moncuquet, M., Hoang, S., 1995. Temperature inversion in the Io plasma torus. Icarus 116, 202–213.

Miller, K., Becker, K., 1987. Ultraviolet and visible fluorescence produced by controlled electron impact on SO_2. Can. J. Phys. 65, 530–534.

Oliversen, R.J., Retherford, K., Bagenal, F., Ballester, G., Feldman, P., Harris, W., McGrath, M., Roesler, F., Scherb, F., Schneider, N., Smyth, W., Trafton, L., Trauger, J., Woodward, R., Wolven, B., Brown, M., 2000. HST/STIS visible sodium and oxygen images of Io in eclipse. EOS Trans. AGU 81. Abstract S290.

Oliversen, R.J., Scherb, F., Smyth, W.H., Freed, M.E., Carey Woodward, R., Marconi, M.L., Retherford, K.D., Lupie, O.L., Morgenthaler, J.P., 2001. Sunlit Io atmospheric [OI] 6300A emission and the plasma torus. J. Geophys. Res. 106, 26183–26194.

Porco, C., West, R., McEwen, A., Del Genio, A., Ingersoll, A., Thomas, P., Squyres, S., Dones, L., Murray, C., Johnson, T., Burns, J., Brahic, A., Neukum, G., Veverka, J., Barbara, J., Denk, T., Evans, M., Ferrier, J., Geissler, P., Helfenstein, P., Roatsch, T., Throop, H., Tiscareno, M., Vasavada, A., 2003. Cassini imaging science at Jupiter. Science 299, 1541–1547.

Radebaugh, J., McEwen, A., Milazzo, M., Keszthelyi, L., Davies, A., Turtle, E., Dawson, D., 2003. Observations and temperatures of Io's Pele Patera from Cassini and Galileo spacecraft images. Icarus. In press.

Rages, K., Beebe, R., Senske, D., 1999. Jovian stratospheric hazes: the high phase angle view from Galileo. Icarus 139, 211–226.

Retherford, K.D., Bagenal, F., Ballester, G., Belton, M., Combi, M., Feldman, P., Harris, W., McGrath, M., Moos, H., Oliversen, R., Roesler, F., Scherb, F., Schneider, N., Smyth, W., Stern, A., Trafton, L., Trauger, J., Woodward, R., Wolven, B., 1999. HST-Galileo Io campaign: images of sodium and oxygen emissions in eclipse. EOS Trans. AGU 80 (46). Fall Meet. Suppl. F621.

Retherford, K.D., Moos, H.W., Strobel, D.F., Wolven, B.C., Roesler, F.L., 2000. Io's equatorial spots: morphology of neutral UV emissions. J. Geophys. Res. 105, 27157–27166.

Roesler, F.L., Moos, H.W., Oliversen, R.J., Woodward, R.C., Retherford, K.D., Scherb, F., McGrath, M.A., Smyth, W.H., Feldman, P.D., Strobel, D.F., 1999. Far-ultraviolet imaging spectroscopy of Io's atmosphere with HST/STIS. Science 283, 353–357.

Saur, J., Neubauer, F.M., Strobel, D.F., Summers, M.E., 1999. 3D plasma simulations of Io's interaction with the Io plasma torus: asymmetric plasma flow. J. Geophys. Res. 104, 25105–25126.

Saur, J., Neubauer, F.M., Strobel, D.F., Summers, M.E., 2000. Io's ultraviolet aurora: remote sensing of Io's interaction. Geophys. Res. Lett. 27, 2893–2895.

Saur, J., Neubauer, F.M., Strobel, D.F., Summers, M.E., 2002. Interpretation of Galileo's Io plasma and field observations: the I0, I24, I27 flybys, and close polar passes. J. Geophys. Res. 107 (A12). 1478, 5-1–5-18.

Saur, J., Neubauer, F.M., Strobel, D.F., Summers, M.E., 2003. The ion mass loading rate at Io. Icarus 163, 456–468.

Scherb, F., Smyth, W., 1993. Variability of (O I) 6300-a emission near Io. J. Geophys. Res. 98, 18729–18736.

Schneider, N.M., Hunten, D.M., Wells, W.K., Schultz, A.B., Fink, U., 1991. The structure of Io's corona. Astrophys. J. 368, 298–315.

Schneider, N.M., Park, A.H., Kuppers, M.E., 2000. Spectroscopic studies of the Io torus during Galileo encounters: remote plasma diagnostics and the detection of Cl^{++}. In: AAS/Division for Planetary Sciences Meeting 32nd, Pasadena, CA. Abstract 35.03.

Spencer, J.R., Jessup, K.L., McGrath, M.A., Ballester, G.E., Yelle, R.V., 2000. Discovery of gaseous S_2 in Io's Pele plume. Science 288, 1208–1210.

Strobel, D.F., Wolven, B.C., 2001. The atmosphere of Io: abundances and sources of sulfur dioxide and atomic hydrogen. Astrophys. Space Sci. 277, 271–287.

Trauger, J.T., Stapelfeldt, K.R., Ballester, G.E., Clarke, J.T., WFPC2 Science Team, 1997. HST Observations of [OI] Emissions from Io in Eclipse. In: American Astronomical Society, DPS meeting #29. Abstract #18.02.

Vatti Palle, P., Ajello, J., Bhardwaj, A., 2004. The high resolution far ultraviolet spectrum of electron-excited SO_2. J. Geophys. Res. 109 (A2). A02310.

West, R.A., 1988. Voyager 2 imaging eclipse observations of the jovian high altitude haze. Icarus 75, 381–398.

Zatsarinny, O., Tayal, S.S., 2002. Electron impact collision strengths and rates for neutral sulphur using the *B*-spline *R*-matrix approach. J. Phys. B: At. Mol. Opt. Phys. 35, 2493–2503.